

there is a strong absorption band near 52 microns at both temperatures. Furthermore, there is also high absorption beyond 100 microns at 297°K. This is borne out by the transmission curves shown in Fig. 1. The sample is nearly intrinsic with  $n=p=2.4 \times 10^{16}$   $\text{cm}^{-3}$  at 297°K, while  $p \sim 10^{15}$   $\text{cm}^{-3}$  and  $n \ll 10^{15}$   $\text{cm}^{-3}$  at 78°K. The 52-micron band is thus independent of the carrier concentration and is therefore a lattice band. The high absorption beyond 100 microns, observed at 297°K seems to be caused by the carriers,<sup>1</sup> since the absorption becomes small at 78°K.

Reflectivity measurements at 297°K on an  $n$ -type sample of  $n=10^{17}$   $\text{cm}^{-3}$  and a  $p$ -type sample of  $p=10^{17}$   $\text{cm}^{-3}$  confirm the above interpretation. The same 52-micron band is present in both samples. Beyond 100 microns, the  $n$ -type sample shows an even higher reflectivity than the pure sample at 297°K while the  $p$ -type sample has the low reflectivity shown by the pure sample at 78°K. Thus we see that the high re-

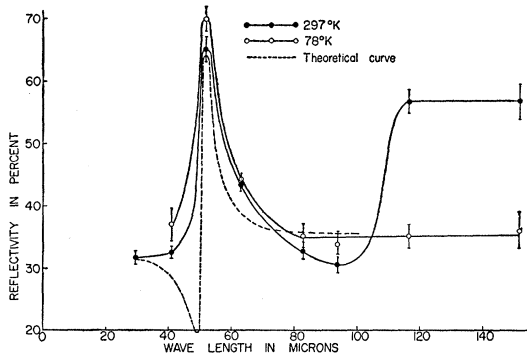


FIG. 2. Reflectivity as a function of wavelength for an InSb sample;  $N_A=10^{16}$   $\text{cm}^{-3}$ .

fectivity at long wavelengths is caused by absorption due to the conduction electrons.

The strong lattice band near 52 microns indicates some degree of ionic binding. This absorption gives a contribution to the complex susceptibility,

$$\alpha = \frac{\Delta\epsilon_s \omega_0^2}{4\pi(\omega_0^2 - \omega^2) + i\gamma\omega},$$

where  $\Delta\epsilon_s$  is the contribution to the static dielectric constant. By comparing the reflectivities on the short- and long-wavelength sides of this band we estimate  $\Delta\epsilon_s < 1.5$ . The dashed curve (Fig. 2) was calculated with  $\omega_0 = 3.5 \times 10^{13}$   $\text{sec}^{-1}$  and  $\gamma = 1.3 \times 10^{12}$   $\text{sec}^{-1}$ , and the limiting value  $\Delta\epsilon_s = 1.5$  was used to get the high reflectivity. The discrepancy between this curve and the curve measured at 78°K may be due to poor resolution. In fact, the measurements at 52 microns were made with three NaCl and an InSb crystals as residual ray plates; with four NaCl plates the measured reflectivity was  $\sim 50\%$  instead of 65%. These observations confirm the narrowness of the reflection band in

InSb. Using the expression<sup>2</sup>

$$\Delta\epsilon_s = \frac{4\pi N e^{*2} (n^2 + 2)^2}{M\omega_0^2 3},$$

where  $M$  is the reduced mass of the atoms and  $n$  is the short-wavelength refractive index, the effective ionic charge is estimated to be  $e^* = 0.34e$ .

The question arises whether partial ionic binding would be compatible with the high carrier mobilities observed. The formula of mean free path for polar scattering<sup>3</sup> has been derived for  $kT \ll \hbar\omega_l$ , where  $\omega_l$  is the frequency of longitudinal waves. At 80°K,  $\hbar\omega_l = 3.4kT$ , this gives a mobility

$$\mu_{\text{polar}} = -\frac{e}{m} \left( \frac{3kT}{m} \right)^{-\frac{1}{2}} \frac{6}{\sqrt{\pi}} \frac{n^2(n^2 + \Delta\epsilon)}{\Delta\epsilon} \left( \frac{kT}{\hbar\omega_l} \right)^{\frac{1}{2}} \\ \times \left[ \exp\left( \frac{\hbar\omega_l}{kT} \right) - 1 \right] \left( \frac{m}{m^*} \right)^{\frac{3}{2}} \approx 15000 \left( \frac{m}{m^*} \right)^{\frac{3}{2}} \frac{\text{cm}^2}{\text{volt sec}}.$$

This is higher than the mobilities observed around this temperature for holes as well as electrons, the latter having a small effective mass.

It is interesting to note that the transmission up to 35 microns decreased with decreasing temperature within the extrinsic range; at 297°K the sample is intrinsic. As reported previously,<sup>4</sup> in samples with  $N_A \geq 10^{17}$   $\text{cm}^{-3}$  the transmission decreases steadily from 297°K down.

This work was stimulated by some preliminary reflection measurements made by E. J. Johnson at the suggestion of Professor K. Lark-Horovitz.

\* Work supported by a Signal Corps Contract.

<sup>1</sup> H. Y. Fan and M. Becker, *Symposium Volume of the Reading Conference* (Butterworth Publishing Company, London, 1951).

<sup>2</sup> H. Fröhlich, *Theory of Dielectrics* (Clarendon Press, Oxford, 1949).

<sup>3</sup> Fröhlich, Pelzer, and Zienau, *Phil. Mag.* **41**, 211 (1950).

<sup>4</sup> W. Kaiser and H. Y. Fan, *Phys. Rev.* **98**, 966 (1955).

## Experimental Evidence for Dislocations in Crystalline Quartz

H. E. BÜMMEL, W. P. MASON, AND A. W. WARNER, JR.

*Bell Telephone Laboratories, Murray Hill, New Jersey*

(Received July 26, 1955)

RECENT measurements of well etched, mounted, and contoured  $AT$  shear vibrating quartz crystals, shown by Fig. 1, indicate that the  $Q$  decreases inversely proportional to the frequency up to 100 Mc/sec. This result is indicative of a relaxation. To verify the existence of such a relaxation, measurements of internal friction of single crystals have been made from 1.5°K to 300°K and in the 5- to 80-Mc/sec frequency region. The results for a 5-Mc/sec crystal are shown by Fig. 2.

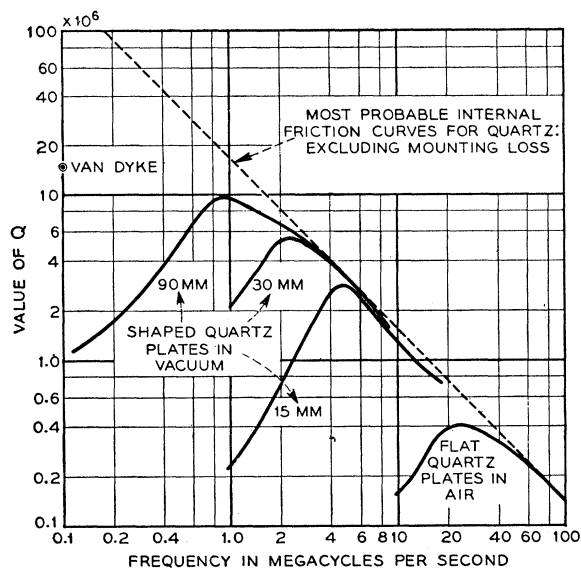


FIG. 1. Experimental measurements of  $Q$  of  $AT$  quartz crystals as a function of frequency and size. Dashed line indicates most probable internal friction as a function of frequency for quartz alone.

As can be seen,  $Q^{-1}$  increases as the temperature decreases, shows two maxima and then drops to a low value which is thought to be determined by the mounting loss. The internal friction, as shown by the dashed lines, can be divided into three parts labeled mounting loss, dislocation relaxation, and oxygen vibrations.

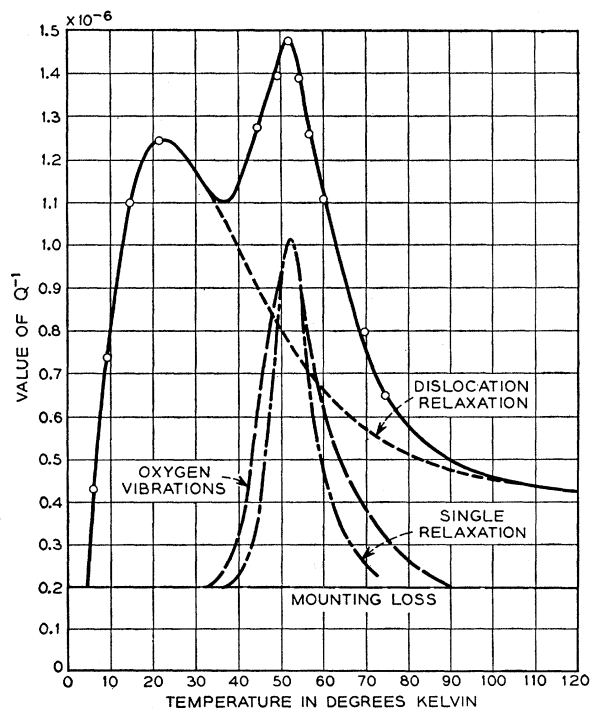


FIG. 2. Internal friction for a 5-Mc/sec  $AT$  quartz crystal as a function of temperature.

To justify this division, measurements were made for a number of crystals whose frequencies ranged from 5 to 80 Mc/sec. In every case two peaks were obtained and Fig. 3 shows a plot of the relaxation frequencies against  $1/T$ . There are two relaxation frequencies determined by the equations of Fig. 3. The high-energy curve agrees well with one measured previously in fused silica.<sup>1</sup> This peak is thought to be due to impurities distorting the lattice until it approximates the fused silica lattice in the neighborhood of the impurities. The height of the peak is from 1/2000 to 1/20 of the height of the fused silica peak and the relaxation spectrum is much narrower indicating only a small range of bond angles.

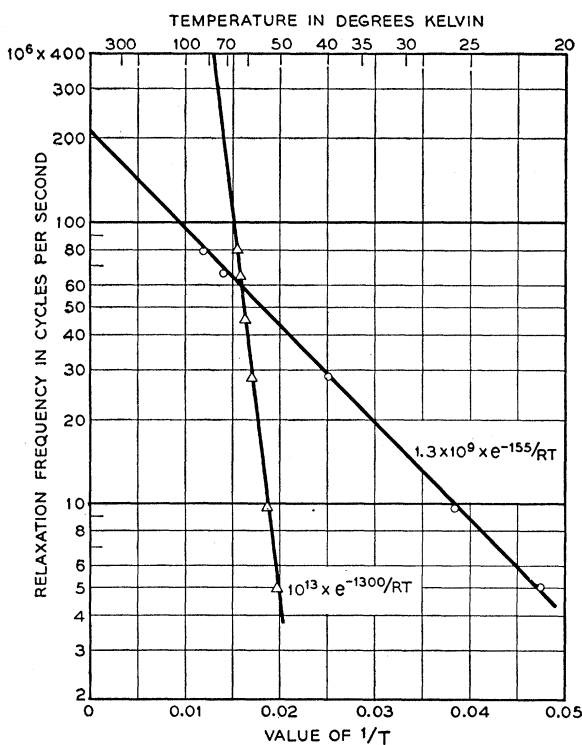


FIG. 3. Semilogarithmic plot of relaxation frequencies as a function of  $1/T$ .

The lower activation energy curve is thought to be caused by dislocations. The relaxation peak is similar to that found in metals.<sup>2</sup> This has been attributed to pinned dislocations being displaced from their minimum energy position by one atomic spacing in the glide plane. Another characteristic of dislocation loss is the exponential increase at high temperatures due to breakaway of dislocations from their impurity pinning points. This type of loss in quartz, occurring at high temperatures, is shown by the work of Cook and Breckenridge.<sup>3</sup> From these data and the theoretical equations of reference 2, one finds values for dislocation

number, loop length, and ratio of limiting shear stress to elastic shear modulus compared with a metal in Eq. (1).

	$\bar{N}$ disloc. per cm <sup>2</sup>	Loop length in cm	Ratio of ( $T_{13}$ ) <sub>0</sub> /μ	(1)
Metal	10 <sup>5</sup> to 10 <sup>6</sup>	4×10 <sup>-4</sup>	5 ×10 <sup>-6</sup>	
Quartz	10 <sup>8</sup>	2×10 <sup>-3</sup>	4.5×10 <sup>-8</sup>	

The lower value of ( $T_{13}$ )<sub>0</sub>/μ indicates that the dislocations are broader than those in metals. The lower number of dislocations present accounts for the smaller dissipation and greater mechanical stability of quartz. The small residual aging of the elastic properties of quartz noted after processing the crystal is probably due to the stabilizing of dislocation positions as a function of time. This aging should be eliminated if the crystal is held at a very low temperature.

<sup>1</sup> See O. L. Anderson and H. E. Bömmel, *J. Am. Ceram. Soc.* **38**, No. 4 (April, 1955).

<sup>2</sup> W. P. Mason, *Phys. Rev.* **98**, 1136 (1955).

<sup>3</sup> R. K. Cook and R. G. Breckenridge, *Phys. Rev.* **92**, 1419 (1951); see Fig. 2.

## Dynamics of Rarefied Gases\*

MAX KROOK

*Harvard College Observatory, Cambridge, Massachusetts*

(Received July 21, 1955)

**B**HATNAGAR, Gross, and Krook<sup>1</sup> have proposed a model for the statistical representation of molecular collisions in gases. The model leads to nonlinear kinetic equations which incorporate the same essential physical properties as the Boltzmann equation but are mathematically more tractable. Linearized forms of the equations have been used to study small-amplitude oscillations in gaseous systems.<sup>1,2</sup>

For several boundary-value problems of one-dimensional steady flow, exact numerical solutions of the full nonlinear equations can be obtained without excessive labor. In such problems with simple gases, the state of a system is specified by a distribution function  $f(\mathbf{v}, x)$ , where  $x$  = position coordinate and  $\mathbf{v} = (v_1, v_2, v_3)$  = molecular velocity. Let  $m$  = molecular mass,  $n(x)$  = number density,  $\mathbf{q}(x)$  = flow velocity,  $T(x)$  = kinetic temperature, and  $c(x) = [kT(x)/m]^{1/2}$  ( $k$  = Boltzmann's constant). In the absence of external forces, the kinetic equation is then<sup>1</sup>:

$$v_1 \partial f / \partial x = -n\kappa f + n^2 \kappa \Phi(\mathbf{v}; \mathbf{q}(x), c(x)) \quad (1)$$

with

$$\Phi(\mathbf{v}; \mathbf{q}, c) \equiv (2\pi c^2)^{-3} \exp[-(\mathbf{v} - \mathbf{q})^2 / 2c^2]; \quad (2)$$

$n\kappa$  is the collision frequency; we have taken  $\kappa$  independent of  $\mathbf{v}$  or equal to some average over  $\mathbf{v}$ . (Kinetic equations corresponding to more general models<sup>2</sup> can also be used in this work.)

Introducing  $\tau = \int n\kappa dx$  as independent variable in

place of  $x$ , we can write (1) in the form:

$$\frac{\partial}{\partial \tau} (e^{\tau/v_1} f) = \frac{e^{\tau/v_1}}{v_1} n(\tau) \Phi(\mathbf{v}; \mathbf{q}(\tau), c(\tau)). \quad (3)$$

The variable  $\tau$  is analogous, in some respects, to the optical depth of radiative transfer theory (for an excellent account of that theory, see Kourganoff<sup>3</sup>).

To handle boundary-value problems it is usually necessary to use the functions  $f_{\pm}$  which represent  $f(\mathbf{v}; \tau)$  in the half-spaces  $v_1 > 0$  and  $v_1 < 0$  respectively. Conditions at the boundaries  $\tau = a, b$ , ( $a < b$ ), are determined by physico-chemical considerations. One common type of boundary condition is represented by

$$\begin{aligned} f_+(\mathbf{v}, a) &= A \cdot \Phi(\mathbf{v}; \mathbf{q}_1, c_1), \\ f_-(\mathbf{v}, b) &= B \cdot \Phi(\mathbf{v}; \mathbf{q}_2, c_2), \end{aligned} \quad (4)$$

where the constants  $\mathbf{q}_1, \mathbf{q}_2, c_1, c_2$  are given and  $A, B$  are to be determined. Various other forms of boundary condition also have to be considered, e.g., specular reflection, etc.

Directly from (3), (4), we find explicit expressions for  $f_{\pm}(\mathbf{v}, \tau)$  as integrals involving  $n, \mathbf{q}, c$  and  $A, B$ . Multiplying these solutions successively by 1,  $\mathbf{v}, (\mathbf{v} - \mathbf{q})^2$  and integrating with respect to velocity, we obtain a set of integral equations which suffice to determine the unknowns  $n(\tau), \mathbf{q}(\tau), c(\tau), A, B$ , and hence also  $f(\mathbf{v}, \tau)$ . The integral equations can be solved numerically by a process of successive approximations which, in general, converges rapidly. Problems with different forms of boundary condition can be handled in an analogous way.

Given a *form* for the microscopic boundary conditions, the model enables us to give a unified and consistent treatment of particular flow problems over the complete ranges of values of the various dimensionless parameters (Knudsen number, Mach number, etc.), that characterize the flow. We can, for example, trace the changes in detailed character of a flow as we proceed from the continuum regime, through the slip flow and transition regions, to the free molecule regime.

The kinetic model can also be used to provide information on some methodological questions. Various authors, e.g., Mott-Smith,<sup>4</sup> Wang Chang and Uhlenbeck,<sup>5</sup> have solved the Boltzmann equation for some "steep-gradient" problems, but only by approximate methods of unknown accuracy. The same approximation procedures can be applied to our kinetic equation and the results then compared with the corresponding exact solutions obtained in the above way. This provides some insight into the accuracy of the various approximation methods.

Further, the equations of macroscopic gas dynamics can be derived<sup>2</sup> from our kinetic equation by the Chapman-Enskog procedure; explicit values are thereby obtained for the coefficients of viscosity and of heat